Available online at www.sciencedirect.com

ScienceDirect

journal homepage: www.elsevier.com/locate/he

Dynamic performance of an in-rack proton exchange membrane fuel cell battery system to power servers

Li Zhao [a], Jacob Brouwer [a,*], Sean James [b], John Siegler [b], Eric Peterson [b], Aman Kansal [b], Jie Liu [b]

[a] National Fuel Cell Research Center, University of California, Irvine, Irvine, CA 92697, USA
[b] Microsoft, Redmond, WA 98052, USA

ARTICLE INFO

Article history:
Received 25 August 2016
Received in revised form
8 February 2017
Accepted 2 March 2017
Available online 31 March 2017

Keywords:
PEMFC
Steady state
Transient response
Energy storage
Data center

ABSTRACT

To improve the reliability and the energy efficiency of data centers, as well as to reduce infrastructure costs and environmental impacts, we experimentally evaluated in-rack powering of servers with a hybrid 12 kW Proton Exchange Membrane Fuel Cell (PEMFC) and battery system. The steady state and the transient performance of the PEMFC and battery in response to dynamic AC loads and real server loads have been evaluated and characterized. The PEMFC system responds quickly and reproducibly to load changes directly from the server rack. Peak efficiency of 55.2% in a single server rack can be achieved. The effect of fuel cell coolant temperature on the hybrid system transient behavior is also captured and evaluated. The observed PEMFC transient responses obtained from the experiments were used to design the size of the energy storage component for the hybrid system. Simulations and analysis of various types of energy storage devices for the hybrid system were carried out. To provide power to meet the most significant transient demand, energy storage capacity greater than 0.3 kWh is required for all battery types, while only 0.053 kWh capacity is required for the ultracapacitor. During charging, the ultracapacitor uses the shortest amount of time to recover to the original SOC, while the charging duration for the lead acid battery is twice as long as that of the ultracapacitor.

Introduction

Fuel cells are energy conversion devices that generate electricity directly from a gaseous or gasified fuel by electrochemical reactions of fuel and oxidant on opposite electrodes. The direct electrochemical conversion of fuel allows for high fuel-to-electric conversion efficiencies without pollutant emissions. As reliable and environmentally friendly power sources, fuel cell technology is receiving a great deal of recent attention in data center applications. According to the U.S. Department of Energy [1], data center energy consumption doubled from 2000 to 2006, reaching more than 60 billion kWh per year at 2006.

Currently most data centers rely upon utility grid power, so that widespread implementation of fuel cell technologies in data centers could significantly lower the generation

* Corresponding author.
E-mail addresses: jb@nfcrc.uci.edu, jb@apep.uci.edu, jbrouwer@uci.edu (J. Brouwer).
http://dx.doi.org/10.1016/j.ijhydene.2017.03.004

emissions and the overall energy consumption. But, what is the best way to utilize fuel cells in data centers? Recently, eBay Inc. implemented 6 MW of fuel cells from Bloom Energy® in its Utah data center with a grid parallel configuration [2]. The data center uses the grid for dynamic and backup power so that the fuel cells make the data center more reliable and invulnerable to grid blackouts. This is a relatively simple way of utilizing fuel cells as base-loaded, grid parallel (and/or backup) data center power sources.

Instead, we propose a Distributed Fuel Cell (DFC) architecture, a direct generation method that places fuel cells at the rack level inches from servers [3,4]. From the perspective of computer architecture, DFC architecture limits the failure domain to a few dozen servers. Modern software technologies can tolerate such failures through replication and load balancing. As a result of our method, equipment such as power distribution units, high voltage transformers, expensive switchgear, and AC-DC power supplies in servers from data centers could be eliminated [3,4]. In data centers, the operation of servers generates large power changes in a relatively short period of time and the power sources must be able to follow the transient demand. Due to lack of previous studies, questions regarding the dynamic responses and capabilities of a hybrid fuel cell/battery system and the system integration and control required are impeding the implementation of the fuel cell systems to data centers using the DFC architecture [3,4]. To facilitate the implementation of fuel cell systems to data centers, transient analysis of the fuel cell system and energy storage components needs to be carried out with data center load dynamics.

The data center industry has experimented with centralized grid-connected fuel cells through simulation and pilot installations. Such studies and demonstrations are mainly focused on: 1) installing high temperature fuel cells (several MW capacity) to power an entire data center [5,6], 2) advancing combined heat and power technology in the data center for better efficiency [7,8], and 3) performing economic and energy efficiency assessments [8,9]. Manno [7] simulated a cogeneration system based on a natural gas membrane steam reformer producing a pure hydrogen flow for electric power generation in a PEMFC. The study demonstrated that heat is recovered from both the reforming unit and the fuel cell in order to supply the needs of the data center. The possibility of further improving data center energy efficiency adopting DC-powered data center equipment is also discussed. Qu [8] reported a comprehensive performance assessment for a combined cooling, heating and power (CCHP) system with fuel cell in a data center. Data analysis and simulation results demonstrated great advantages of CCHP systems over conventional systems in the data center with regard to energy, environment and economic performance. Hagstotz [9] described the use of a molten carbonate fuel cell for data centers and telecommunication installations supplying cooling and electricity. Few of these published studies address the use of a midsized PEMFC system within the server rack that directly generates power, as is accomplished in the current effort.

One of the concerns of using fuel cells to directly power servers is the load following capability of the fuel cells. Fuel cells themselves are able to respond sufficiently fast to load changes due to their rapid electrochemical reaction rates [10]. Electrochemical reactions and charge transfer processes inside the fuel cell typically have time scales on the order of milliseconds [11]. Since the electrochemistry directly produces the electrical work output, a fuel cell system should be able to achieve rapid load following capability on the same order as that offered by the electrochemical reactions if flow and thermal dynamics can be well managed. The relatively slow response of the fuel processing and fuel/air delivery subsystems produce the main challenges associated with load following. The limitations could result from conservative control techniques or from inherently slow responses of subsystem components, such as flow, thermal, or chemical reaction delays associated with fuel/air processing equipment [11]. The PEMFC system response is fundamentally limited by the performance of the fuel preprocessor and the amount of hydrogen present in the anode compartment [4,12]. During transients it is essential that sufficient hydrogen be maintained in the fuel cell to sustain the fuel cell voltage and avoid damage caused by hydrogen starvation. Fuel starvation in the anode compartment can occur if the fuel is consumed by the electrochemical reactions faster than it can be supplied by the fuel delivery system and/or diffused through the electrodes to the electrochemically active sites. Hydrogen is sustained in the anode compartment by controlling the fuel flow rate in proportion to the amount of consumed hydrogen and a desired fuel utilization [12,13]. Other operating conditions such as feed gas humidity, operation temperature, feed gas stoichiometry, air pressure, fuel cell size and gas flow geometry were also found to affect the dynamic response capabilities of PEMFC [14–17].

Hybrid systems comprised of fuel cell and energy storage devices have been tested and simulated both for stationary and transportation applications [18–25]. Commonly used energy storage systems are various types of batteries and ultracapacitors. To satisfy different energy requirements by this type of hybrid system, the fuel cell is designed to provide the average or steady-state power while the energy storage component provides the transient power or peak power [18,20,23]. Simulation studies aimed to improve the control and energy management of the hybrid system have been carried out by several groups [18,20,24,25]. These studies were focused on the control techniques that regulate the power flow and energy management between the devices.

In this study, we demonstrate and evaluate a direct generation method that places a hybrid power system (comprised of a 12 kW PEMFC system and battery) at the rack level, inches from servers. Recent studies have been carried out to investigate PEMFC system dynamic modeling theoretically [26–32] while few of these published studies have addressed the transient performance of a PEMFC hybrid system that considers both PEMFC and energy storage system to power servers, both experimentally and theoretically as in this effort. The goal of this work is to evaluate the concept and the transient performance of the PEMFC system, and provide insights on the design of energy storage devices for use with PEMFC to power servers. The performance and the dynamic load following capabilities of the PEMFC system and the battery were evaluated and characterized. Further, simulations and analysis of various types of energy storage devices for the hybrid system were carried out.

Experimental setup

To demonstrate server racks powered by an in-rack fuel cell system and to analyze the steady-state and transient performance of fuel cells, a hybrid fuel cell-battery system was designed, installed and tested. In this study, the PEMFC system used was a Hydrogenics HyPM™10 kW Rack (PEMFC system with peak power of 12 kW). The battery component used in the hybrid system was an APC Smart-UPS™ VT™ 15 kV A UPS system (with lead acid batteries). The 12 kW in-rack PEMFC system contained a fuel cell stack (rated at 12 kW, 48VDC), a DC/DC converter (±192VDC), a system controller, and the Balance of the Plant (BOP). In the PEMFC system, ultra high purity H_2 was fed to the anode and ambient air was fed to the cathode. The supply of fuel and air were controlled by respective valves and blowers via the fuel cell controller. To reject the waste heat from the fuel cell power production, an internal water-based cooling circuit took the heat from the stack to a heat exchanger, where the heat was transferred to an external cooling circuit and rejected by a cooling subsystem external to the fuel cell rack using an external chiller [3,4]. Anode and cathode exhausts from the fuel cell stack were removed via a blower in the ventilation system which provides continuous ventilation and under pressure inside the fuel cell system [3,4]. In the hybrid system, the power output of the 12 kW in-rack PEMFC system was first converted to 192VDC and then connected to a 10 kV A, 208VAC L-L UPS system to supply AC power to the servers/load. Since the UPS system could only take 192VDC as input, the 48VDC output from the fuel cell was first converted to 192VDC via the converter [3]. The UPS system converts the fuel cell power to conditioned power for the connected server/load. This AC output configuration was designed for initial evaluation of the battery and the fuel cell hybrid system dynamic response characteristics, but it does not represent any preferred or optimal design of the type of hybrid fuel cell battery system envisioned herein. The hybrid system designed and tested is shown in Fig. 1 and the system schematic is shown in Fig. 2.

The electrical properties of the fuel cell system and the battery system were measured using a Yokogawa® WT1600 digital power meter that sampled at 50 ms (20 times per second) intervals. The hydrogen fuel flow rate was measured using an Alicat® hydrogen flow meter (M-250SOPM-D/CM) with 500 ms resolution. The fuel cell system performance, such as fuel cell coolant temperature, air flow rate, and anode pressure were monitored and recorded with 10 s sampling time via the fuel cell controller. The steady state performance characteristics were measured at various external power set points, allowing the fuel flow rate and coolant temperature to stabilize. The transient response measurements were performed by abruptly changing the external load and measuring the response of the voltage and current of the fuel cell system and the battery. The AC load applied to the hybrid system was controlled by three Chroma® 63803 programmable AC electronic load banks. The load banks were connected in three phase parallel mode running under constant power mode with power factor = 1.0. Total of 9 servers were used in this study and the type of the server was 750 W HP® Proliant SE326M1 with two quadcore CPUs and 98GB of memory.

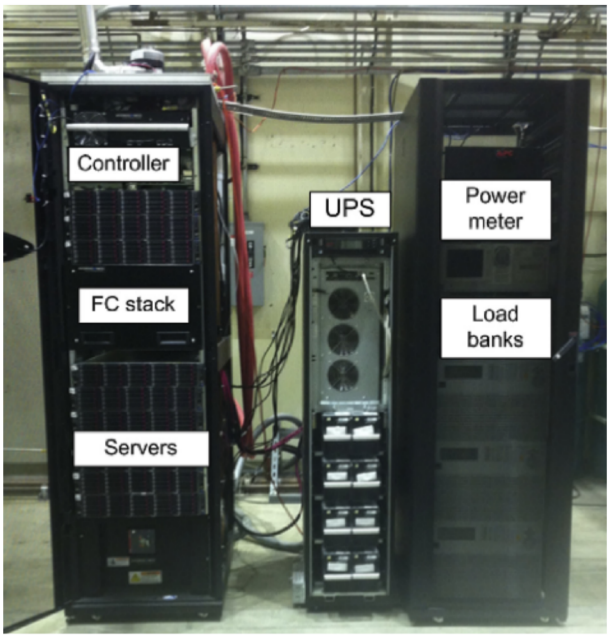

Fig. 1 – The hybrid system tested.

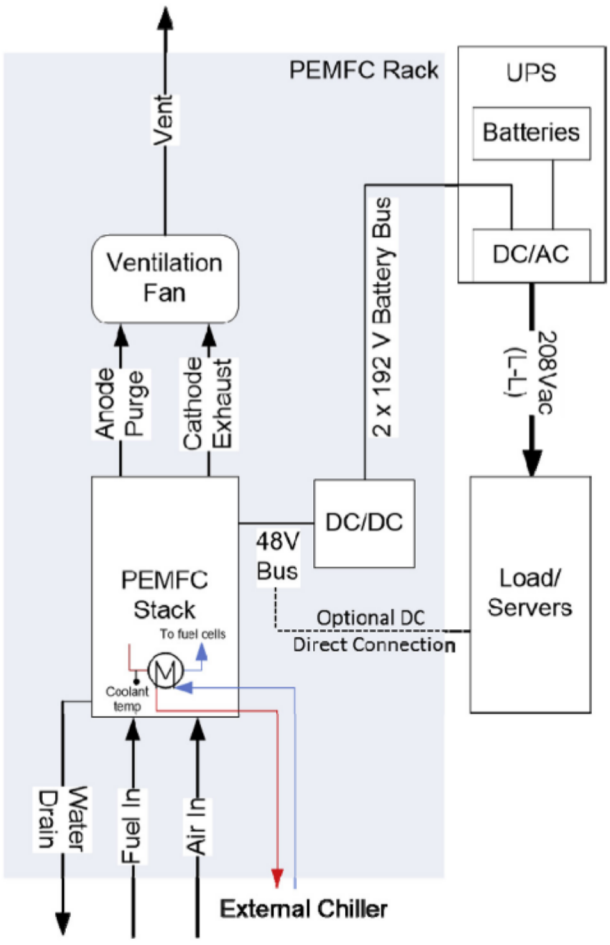

Fig. 2 – The schematic of the hybrid system.

Standard off-the-shelf server power supplies were used to regulate normal current and voltage deviations in the fuel cell stack. The hybrid system designed and tested is shown in Fig. 1 and the system schematic is shown in Fig. 2.

Results and discussion

Steady state performance

The IV polarization curve of the PEMFC system, the maximum voltage disparity amongst cells, the hydrogen flow rate and the air flow rate measured in this study are presented in Fig. 3 with error bars showing the variation in the data. With 60 cells in the PEMFC stack, 55.8 V was observed at open circuit. The average open circuit voltage of the single cell in the stack was measured at 0.93 V. In our test, maximum power of 11.3 kW was achieved and no concentration polarization was observed. The results indicate that when the PEMFC system is operating at peak current levels around 275A, diffusive mass transportation in the electrodes is sufficient and the reactant concentrations are sufficient to avoid concentration polarization. As shown in Fig. 3, the maximum cell voltage disparity increases with the current and becomes relatively stable at around 25 mV. Single cell voltage and the degree of disparity amongst cells shown in Fig. 3 provide important information for the control and monitoring of the stack and system. Operating at high current, the voltages of some cells may decrease compared to the average cell voltage because of small changes in membrane dehydration or fuel depletion disparities amongst the cells [33–35]. The hydrogen and air flow rates are adjusted stoichiometrically with the power so that the reactant and the product ratio can be fixed.

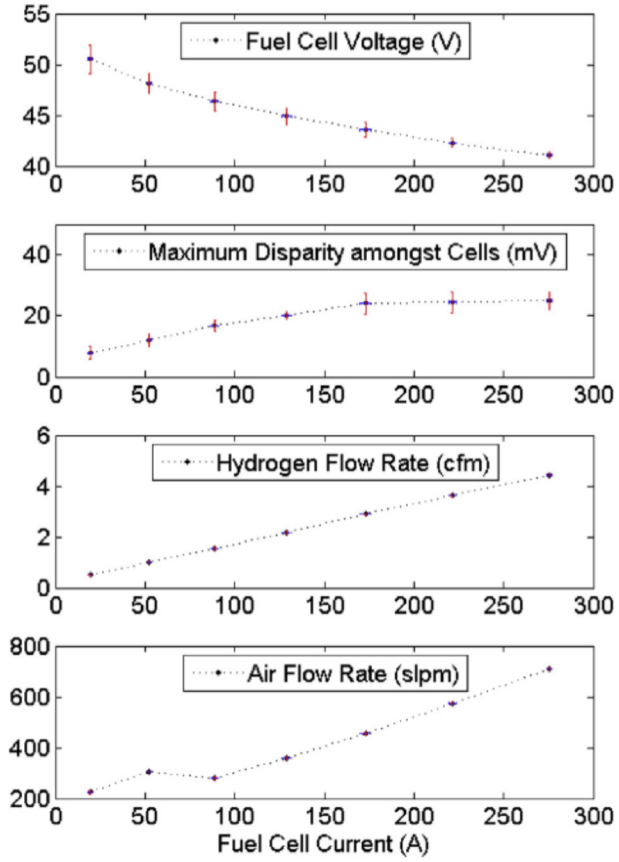

Fig. 3 – Stack I–V polarization curve, maximum voltage disparity amongst cells, hydrogen flow rate, and air flow rate of the 12 kW in-rack PEMFC system. Error bars in the data indicate ± one standard deviation from 5 different measurements.

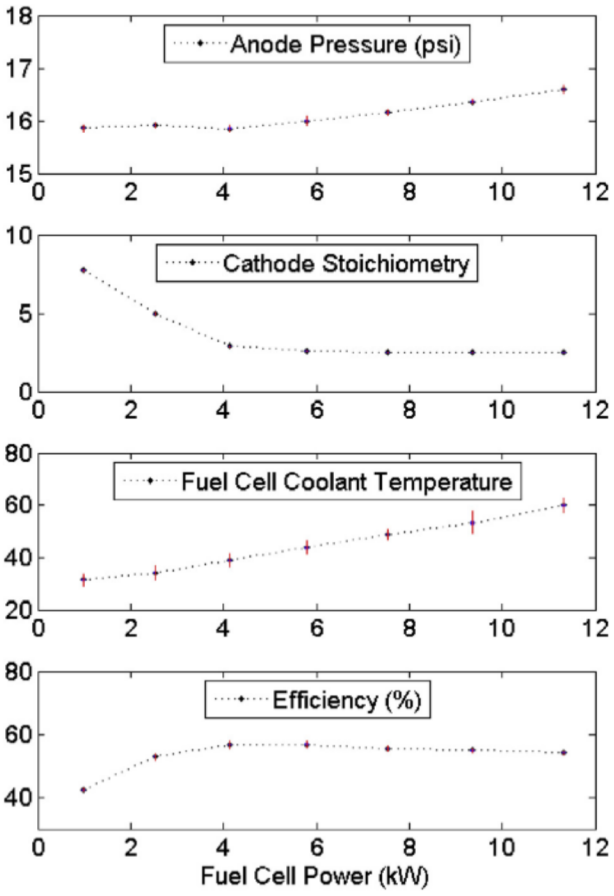

Fig. 4 – Anode pressure, cathode stoichiometry, coolant temperature and fuel cell efficiency of the 12 kW in-rack PEMFC system. Error bars in the data indicate ± one standard deviation from 5 different measurements.

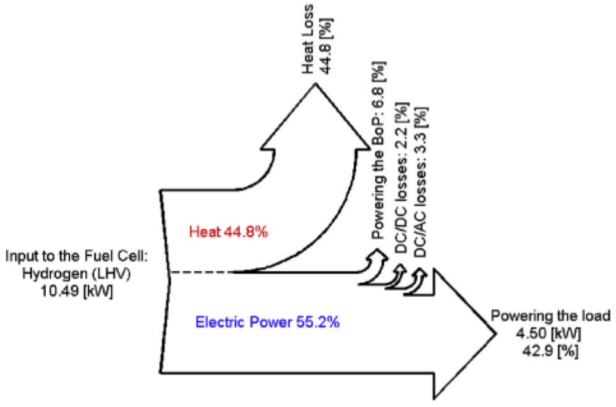

Fig. 5 – Sankey diagram of the PEMFC system operating at 4.5 kW external load.

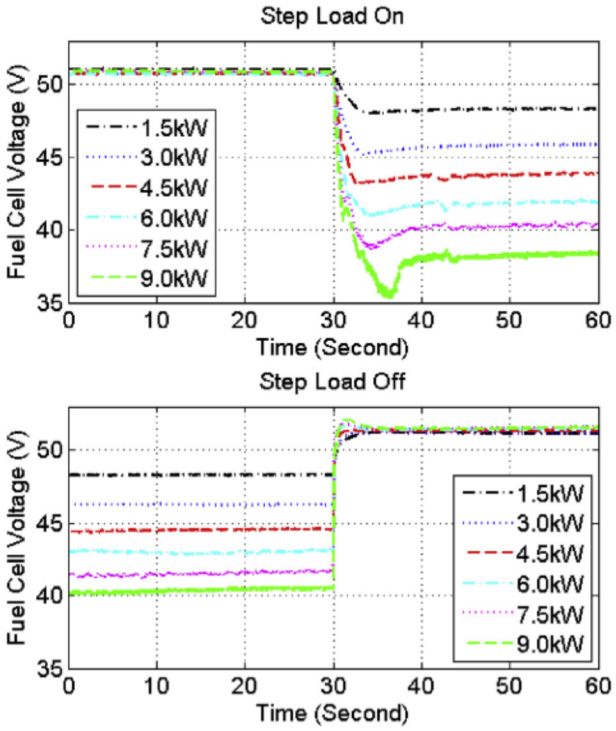

Fig. 6 – Fuel cell voltage responses to various step loads, step loads turned on/off at t = 30 s.

Anode pressure, cathode stoichiometry, fuel cell coolant temperature and fuel cell efficiency of the 12 kW in-rack PEMFC system are presented in Fig. 4 with error bars showing the variation in the data. It is noted that anode pressure increased slightly with the increasing power output. The PEMFC system has relatively high cathode stoichiometry when operating at lower output power, and maintain relatively stable cathode stoichiometry of 2 at higher output power. The fuel cell coolant temperature increases with the output power and remains below 60 °C, suggesting that low grade waste heat was rejected from the PEMFC system. The steady state efficiency of the PEMFC system is calculated using Equation (1) relative to the Lower Heating Value (LHV) of the hydrogen, and takes into account of all on-board parasitic loads [3,4]. System efficiencies were evaluated with various load (0, 1.5 kW, 3 kW, 4.5 kW, 6 kW, 7.5 kW and 9 kW) operating when fuel flow rate and coolant inlet/outlet temperatures were at equilibrium. As shown in the figure, when the fuel cell system output about 50% of its rated power (5 kW), the maximum PEMFC system electrical efficiency will be achieved.

$$\eta_{fc} = \frac{Fuel\ Cell\ Output}{Total\ Hydrogen_{in}(LHV)} \times 100\% \quad (1)$$

To illustrate the energy flow of production and consumption, a Sankey diagram is presented in Fig. 5 for the case when the PEMFC is operating at steady state. As shown in Fig. 5, with the external load of 4.5 kW, the PEMFC system electrical efficiency reaches 55.2% (using the lower heating value of hydrogen). 12.3% of the electric power generated (6.8% of the total energy input) is consumed in the fuel cell balance of plant. A total of 10.0% of the electric power (5.5% of the total energy input) is consumed in the inversion and conversion processes, while 77.7% of the electric power generated (42.9% of the total energy input) is delivered to the load. The results indicate several opportunities to increase the overall system efficiency. Optimizing the balance of plant and reducing the power consumption of the BoP components could further increase the system efficiency. Utilizing the 48VDC output directly from the PEMFC system could also increase the efficiency by eliminating the conversion/inversion losses.

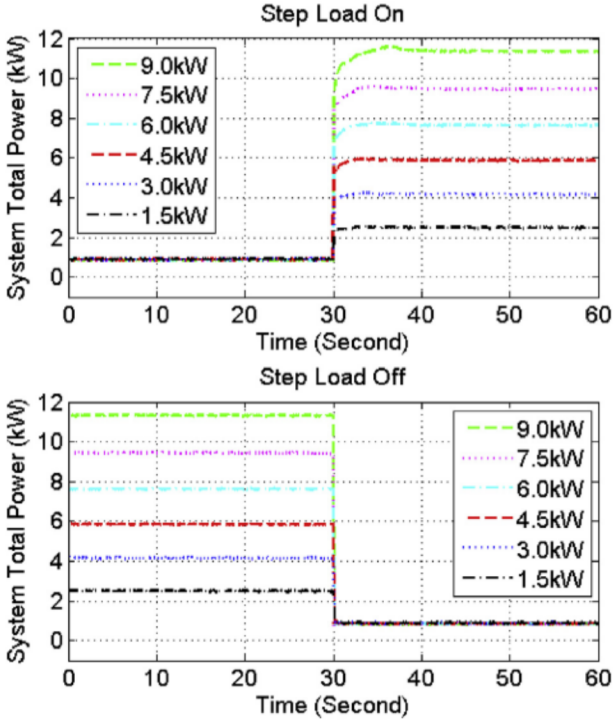

Fig. 7 – Hybrid system power output profiles under various step loads, step loads turned on/off at t = 30 s.

Transient performance with controlled step loads

To evaluate the transient performance of the PEMFC and battery hybrid system, various controlled step loads were applied to the system.

Transient response to step loads

The PEMFC system voltage responses to various step loads are presented in Fig. 6. In the top panel of Fig. 6, starting at t = 0 the PEMFC system was operating at steady state with no external load and at t = 30 s various loads were instantly turned on. In the bottom panel of Fig. 6, starting at t = 0 the PEMFC system was operating at steady state with various loads and at t = 30 s the external loads were instantly turned off. For the cases when the system was undergoing step load increases, the system voltage decreases immediately after the load changes, reaches a minimum value, and then gradually increases (recovers) with time to reach a new steady-state value. Fuel cell voltage undershoot behavior was observed when the loads were stepping up and when they were larger than 1.5 kW. During step load decreases, a corresponding fuel cell voltage overshoot behavior was only observed when the

step load decreases were larger than 4.5 kW. The magnitude of voltage undershoot/overshoot gradually increased with the amount of load change applied. In the case with 9 kW step load increase, during the transient the PEMFC system voltage was undergoing voltage undershoot by up to 3 V (average of 50 mV per cell) and resulted in a longer recovery time to reach a new steady state voltage. It was found that the air flow ratio changes have a significant influence on the cell voltage dynamic response to load change, and the voltage undershoot can be reduced by improving the air stoichiometry change rate or by increasing the initial air stoichiometry [15,36–38].

The total power profiles of the PEMFC and battery hybrid system during load changes were obtained and are presented in Fig. 7, to characterize the dynamic performance of the in-rack hybrid system. As shown in the top panel of Fig. 7, because of the battery in the hybrid system, the system could immediately supply power to meet the step load increases and the PEMFC system ramps up the power gradually within 10 s in all cases. With increasing load change, larger amounts of time are required for the PEMFC system to reach a new steady-state power output. As shown in the bottom panel of Fig. 7, the system power output responds immediately to the load changes when the step loads are turned off.

To further understand the hybrid system transient behavior, high resolution (sampling period = 50 ms) power profiles of both the PEMFC system and the battery during the load change transients were obtained and are presented in Fig. 8 and Fig. 9. The panels of Fig. 8 display the fuel cell and battery transient responses when the external load stepped up from 0 kW to the new power setting (1.5 kW, 3.0 kW, 4.5 kW, 6.0 kW, 7.5 kW and 9.0 kW) at t = 30 s. The panels of Fig. 9 show the fuel cell and battery transient responses when the external load is stepped down from the power setting to 0 kW at t = 30 s. In all step load increase cases, the battery in the hybrid system immediately supplies the power to meet the step load and decreases after the fuel cell starts ramping up. During the largest step load transient from 0 kW to 9.0 kW, as shown in Fig. 8, it took 4.7 s for the PEMFC system to ramp up and fully meet the 9 kW external load. The peak power of the battery was 7.52 kW and total energy needed from the battery was 0.003 kWh. Total energy, average power and peak power required from the battery during transient operation under various load changes are summarized in Table 1. These results provide important insights into the battery sizing and cost optimization regarding the design of the hybrid system for data centers. It is also noted that fuel cell power overshoot is more prominent in the larger step load increase transient. The extra power from the overshoot will charge the battery slightly as shown in Fig. 9. In all step load increase cases, the fuel cell power recovered to the new steady state power within 10 s after the transient demand increase.

The hydrogen flow rates during the load changes were obtained and are presented in Fig. 10 and Fig. 11. As shown in these figures, the hydrogen flow rate varies according to the

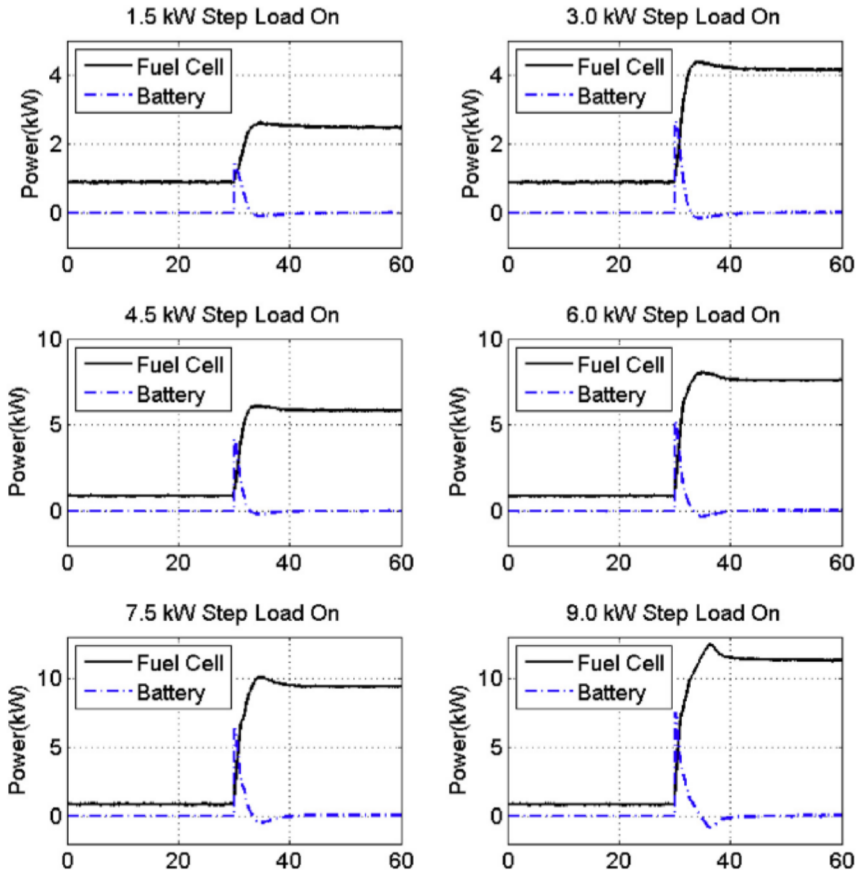

Fig. 8 – The power profiles of the PEMFC system and the battery during transient (step load on).

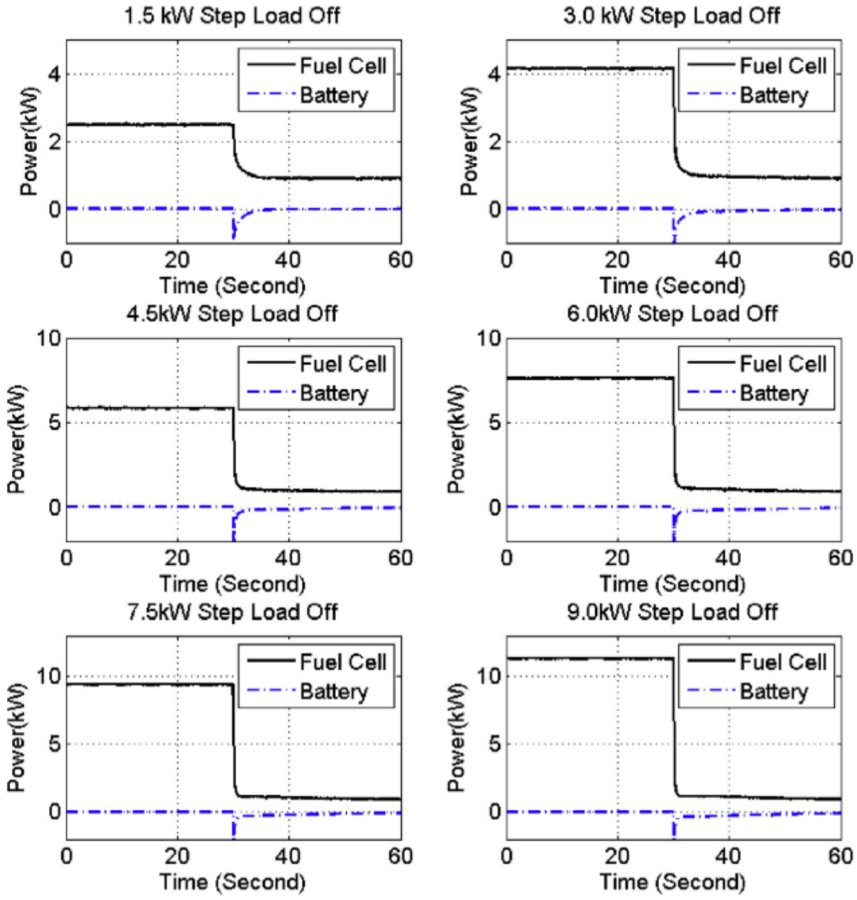

Fig. 9 – The power profiles of the PEMFC system and the battery during transient (step load off).

Table 1 – Energy and average power required from the battery during transient.

External load (kW)	Energy required from battery during transient (kWh)	Average battery power required during transient (kW)	Peak power (kW)
1.5	0.0006	0.5817	1.4192
3	0.0009	1.1507	2.6879
4.5	0.0013	1.5530	4.1774
6	0.0017	1.8169	5.3136
7.5	0.0022	2.3172	6.3865
9	0.0030	2.2915	7.5176

PEMFC system power requirement. The main factors that affect the hydrogen flow rate transient behavior shown in Fig. 10 are the hydrogen fuel delivery control system, and the fuel diffusion through the electrodes to the electrochemically active sites [39]. As the step load increases, the more significant hydrogen flow rate overshoot transient behavior is observed. This overshoot is the result of the fuel delivery control system dynamic intended to always provide sufficient hydrogen to sustain the fuel cell voltage and avoid damage caused by hydrogen starvation during large step changes [40].

Transient response to step loads at various coolant temperature

In this study, an interesting and unique transient behavior of the hybrid system was observed and captured. As shown in Fig. 12, with external load stepped up from 0 kW to 9 kW the PEMFC system power responses varied significantly depending upon the fuel cell coolant temperature. An internal water-based cooling circuit takes the heat from the stack to the internal heat exchanger, where the heat is transferred to an external cooling circuit. The coolant temperature shown is the internal cooling loop outlet temperature (return temperature after the internal cooling loop cools the stack) measured and recorded by the system. The coolant temperature recorded indicates the stack temperature, and the system uses this temperature to control the external cooling circuit flow rate into the internal heat exchanger up to the point of the overheating emergency shutdown set point. It is found that under the same step load change, the PEMFC system power output will oscillate and will require longer time to reach steady state when operating at lower fuel cell coolant temperature. Operating at relatively cold conditions (coolant temperature = 24 °C), the PEFMC system needs 40 s to ramp up to the maximum power and a total of 50 s to reach steady power output. Operating at higher coolant temperatures (e.g., 46 °C), the PEMFC system is able to ramp up from 0.9 kW to 12.1 kW within 5.1 s and achieve steady power output only 9 s after the transient. It is noted that the stack temperature is not available due to the limitation of test. However, the coolant temperature is directly indicative of the operating temperature of the PEMFC system at the beginning of each transient test and since the electrical response times of the stack are much

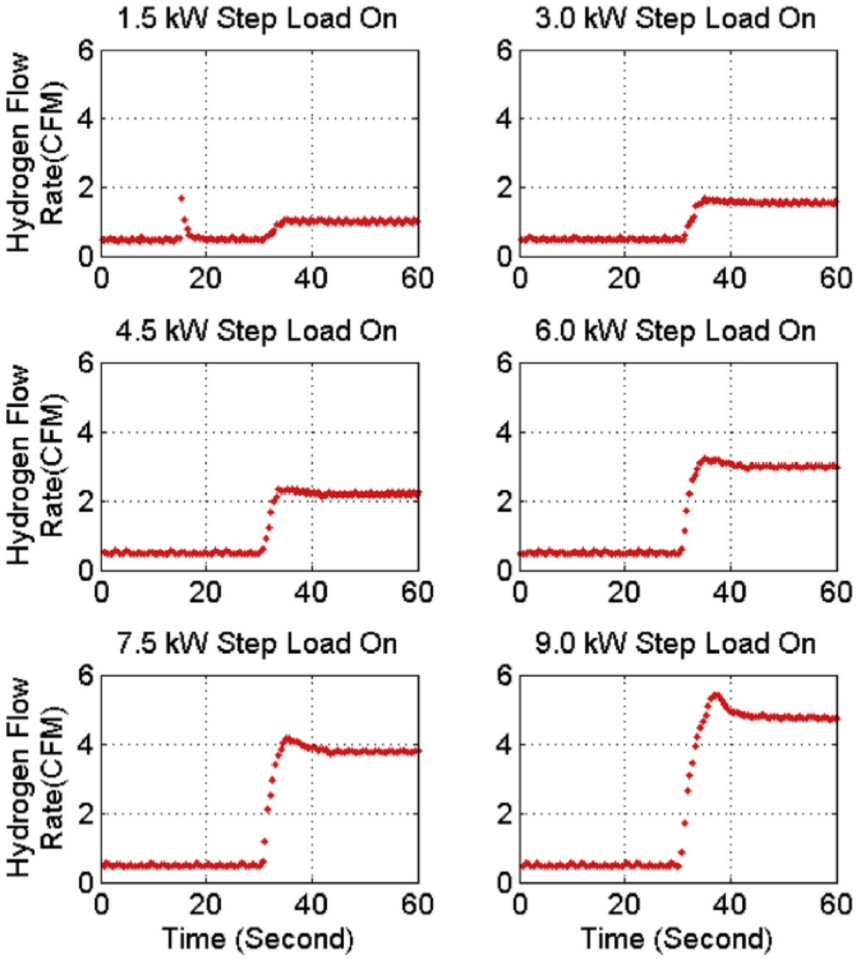

Fig. 10 – The hydrogen flow rate of the PEMFC system and the battery during transient, various step loads turned on at t = 30 s.

shorter than the thermal response times, they are also indicative of the operating stack temperature throughout the transient. The PEMFC operating temperature has a significant impact on the cell and stack dynamic response characteristics. Nernst potential, electrochemical losses and various transport properties (e.g., ionic conductivity of the membrane, the diffusivities of fuel and air constituents, etc.) are all dependent upon operating temperature [41–44]. As shown in Fig. 12, the PEMFC dynamic performance increases with increasing operating temperature. It is likely that the fuel cells have higher polarization losses and can dynamically generate less power when operating at lower temperature. During the 9 kW load change transient with relatively low initial operating temperature, the PEMFC system tends to have less power output than the rated power at steady state. Therefore it is observed that the PEMFC system gradually ramps up the power in the oscillating manner that is monotonically increasingly limited as temperature is decreased. It's also possible that this oscillating behavior at lower coolant temperature is due to the embedded system control strategy that waits for the stack temperature to rise before gradually ramping up the set-points [39]. In addition, at lower temperature, there is a higher propensity for flooding. Therefore the oscillation observed in fuel cell power may also due to the transient blockage by the water in the gas flow channels.

The power profiles of the battery with the PEMFC system operating at various coolant temperatures are shown in Fig. 13. The battery in the hybrid system is designed to dispatch power when the PEMFC system could not fully meet the load during transient. Therefore in the cases when the PEFMC power output is oscillating and gradually ramps up to the peak power as shown in Fig. 12 for the lower temperature cases, the battery has to dispatch in a similar oscillating manner and gradually decrease the power output as shown in Fig. 13. The total amount of energy, average power and peak power required for the battery during these transients are obtained and summarized in Table 2. It is noted that a 9 kW load change transient that occurs at lower operating temperature requires significantly more energy from the battery than the high operating temperature cases. The voltage responses and the hydrogen flow rates of the PEMFC system operating at various coolant temperatures are presented in Fig. 14 and Fig. 15. As shown in the figures, the power profiles are corresponding to the voltage profiles of the PEMFC system, and the hydrogen flow rate varies according to the PEMFC system power output. As indicated from the transient behavior

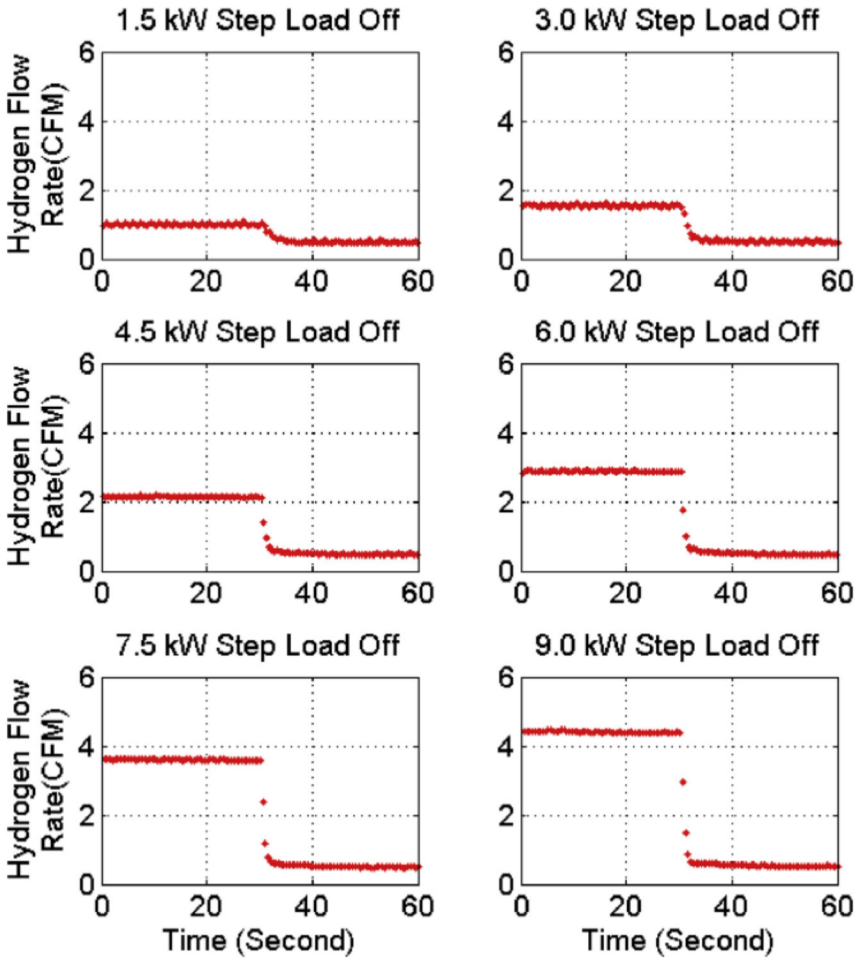

Fig. 11 – The hydrogen flow rate of the PEMFC system and the battery during transient, various step loads turned off at t = 30 s.

showed, larger battery capacity is required if the hybrid system has meet large load demand increases at relatively low operating temperature.

Transient response to server load

To evaluate the dynamic behavior of the PEMFC and battery hybrid system, server loads were also applied to the system. In this test, servers (HP® Proliant SE326M1) were connected to the hybrid system output (120VAC, L-N) through a power distribution unit. Dynamic operations of the servers were performed and the responses of the fuel cell voltage/power, battery power and total system output power were measured.

Cold start

To evaluate the startup behavior of the in-rack hybrid system, a cold start test was performed. 9 servers were kept running at normal work load as powered by the grid, and at a certain time point the grid power was disconnected; at which time the hybrid system was automatically turned on and started to supply power to the servers to keep them operating. The battery power output, the PEMFC system voltage response and the hydrogen flow rate in the cold start process are presented in Fig. 16. As shown in the figure, grid power was disconnected and the hybrid system started at t = 30 s. The battery in the hybrid system immediately supplied power to both the servers operation and the PEMFC system initialization. During the PEMFC initialization process, fuel cell components such as fuel cell controller, air blowers, and exhaust blower will draw power from the battery until the PEMFC starts to produce power. As shown in Fig. 16, ~60 s after the hybrid system was turned on, the PEMFC system starts supplying hydrogen to the cells and there was a hydrogen flow rate spike associated with this supply dynamic. As a result, the fuel cell voltage started to increase and eventually achieved the OCV. After about another 30 s, the PEMFC system was able produce current (power) to meet the server load. It is also noted that the battery was being recharged slightly by the excess power output of the PEMFC system. It is demonstrated that the hybrid system designed and tested in this study could be utilized as a backup power supply that would be able to maintain the server operation during a grid power outage.

Server loads

It has been widely studied and reported that data center power consumption has both short and long term dynamic

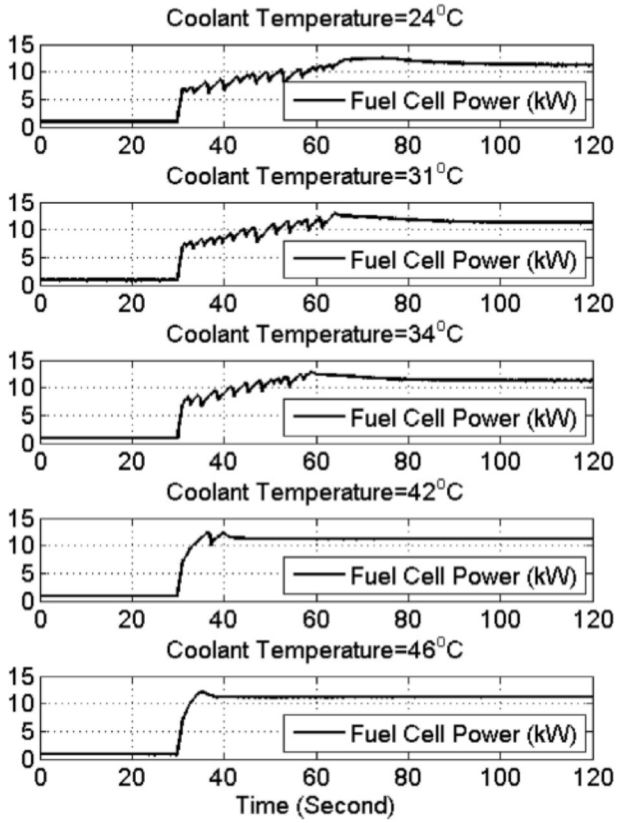

Fig. 12 – The power profiles of the PEMFC system operating at various coolant temperatures, the external load changes from 0 kW to 9 kW at t = 30 s.

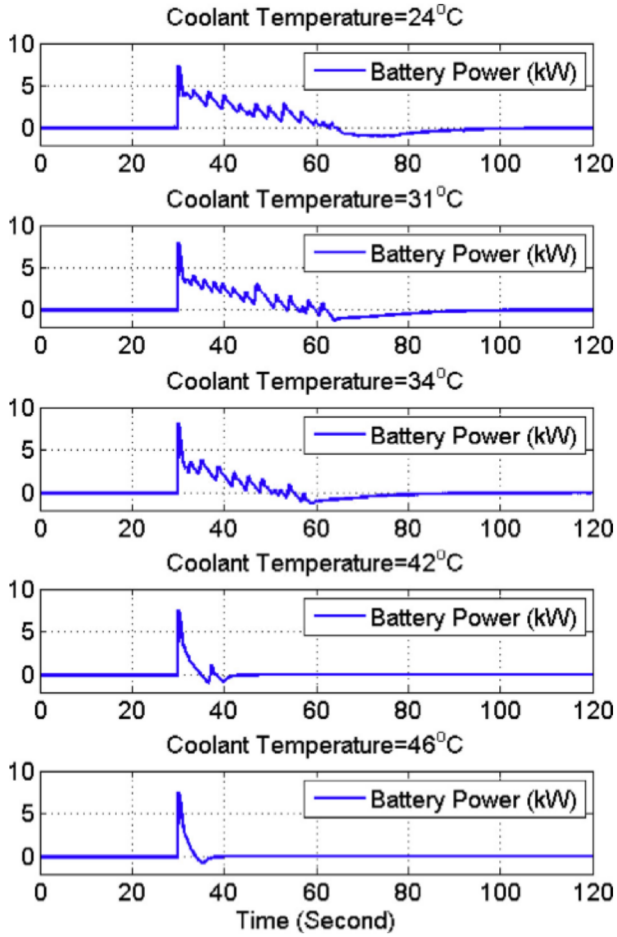

Fig. 13 – The power profiles of the battery with PEMFC system operating at various coolant temperatures, the external load changes from 0 kW to 9 kW at t = 30 s.

variations due to workload fluctuations and server on/off events [3,4]. As demonstrated previously, it usually takes several seconds for the PEMFC system to ramp the power up to meet load increase perturbations. In data center applications when the server has to be cold rebooted, the fuel cell system must be able to follow sudden power demand increases, which may require an external energy storage device such as a battery. Based upon the current experiments with real servers, the only time that the server can cause large and rapid load changes is during the startup or shutdown processes [3,4]. To examine the transient behavior of the hybrid system, real server loads were applied to the system. In the test, multiple servers were turned on when the PEMFC system was running at steady state without any external load. As shown in Fig. 17, the load of the servers changed instantaneously reacting to being turned on producing a highly dynamic power demand increase. Regardless of the number of servers being turned on at once, it took the PEMFC system about the same amount of time (~6 s) to ramp up to the maximum power needed by the server. The battery supplied all the power needed in the instantaneous power spike (which lasts less than 50 ms) caused by the sudden CPU utilization increment. In all three cases, eleven seconds after the servers were turned on, the PEMFC system could follow the server dynamics pretty well. Fig. 18 shows the hydrogen flow rate transient response to the servers' dynamic operations. It's noted that with increasing server loads, the magnitude of hydrogen flow rate overshoot also increased. Total energy, average power and peak power required from the battery during transient operation under various server load changes are summarized in Table 3. Compared to the step load test results presented in section Transient response to step loads, the server loads are more dynamic during transient operation; and as a result, the battery is required to dispatch power to the load more than once. Therefore the maximum battery capacity needs to be carefully evaluated according to the transient response characteristics of the dynamic loads in the server rack.

Energy storage component simulation and capacity analysis

As presented in the previous section, the PEMFC system will require several seconds to ramp power up to meet dynamic load increases and an external energy storage device such as a battery is required. To implement the in-rack power generation application demonstrated in this study for data centers, the sizing and the characteristics of the battery must be evaluated as well as the characteristics of the load changes in server racks and data centers. Data center workload exhibits long term changes over days and weeks, however these changes are typically slower than the fuel cell ramping rates

Table 2 – Battery power and energy need during the transient when PEMFC system operating at various coolant temperatures.

External load (kW)	Coolant temperature (°C)	Energy required from battery during transient (kWh)	Average battery power required during transient (kW)	Peak power (kW)
9	24	0.0203	2.1221	7.3649
	31	0.0154	1.8531	7.9819
	34	0.0113	1.7610	8.1084
	42	0.0033	1.8549	7.5220
	46	0.0027	2.5359	7.5994

[3,4]. Unpredictable events such as rebooting a server in software or server software crashes do not cause any significant power changes. This is due to the electrical components that remain powered in the reboot process. As a result, as long as server load dynamics like those investigated above are met by the fuel cell/battery hybrid system, then it is anticipated that in-rack fuel cell power generation can meet all required power demand dynamics [3,4]. Therefore the most important transient demands that must be considered are the power on and off events. Ideally if the server power on and off events in the rack can be scheduled and staggered over time, a single server sized battery can be utilized and shared by multiple servers in the rack. However, with the consideration of the instantaneous power spike observed during startup and the fuel cell oscillation transient observed, the energy storage component needs to be evaluated and designed accordingly.

There are various types of electrical energy storage technologies that can be used in the hybrid fuel cell system to supply additional power to servers during transient operation. As shown in Fig. 19, ultracapacitors, Li–ion batteries, Lead–acid batteries, Ni–Cd batteries, and Ni–MH batteries are capable of discharge times in minutes with corresponding sizes of 1 kW–100 kW. All of these energy storage devices are well-suited for use with the in-rack fuel cell system. In this section, various energy storage devices including

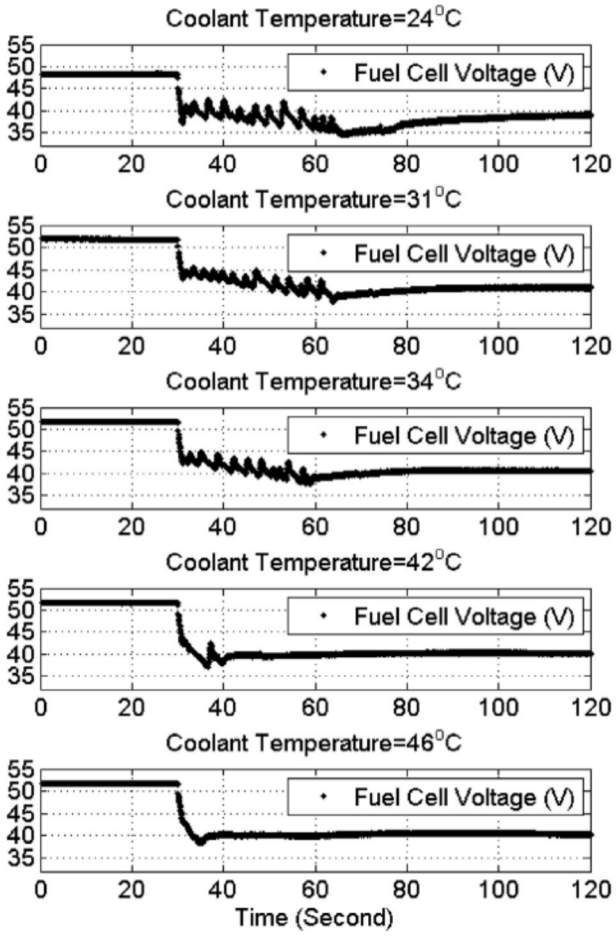

Fig. 14 – The voltage response of the PEMFC system operating at various coolant temperatures, the external load changes from 0 kW to 9 kW at t = 30 s.

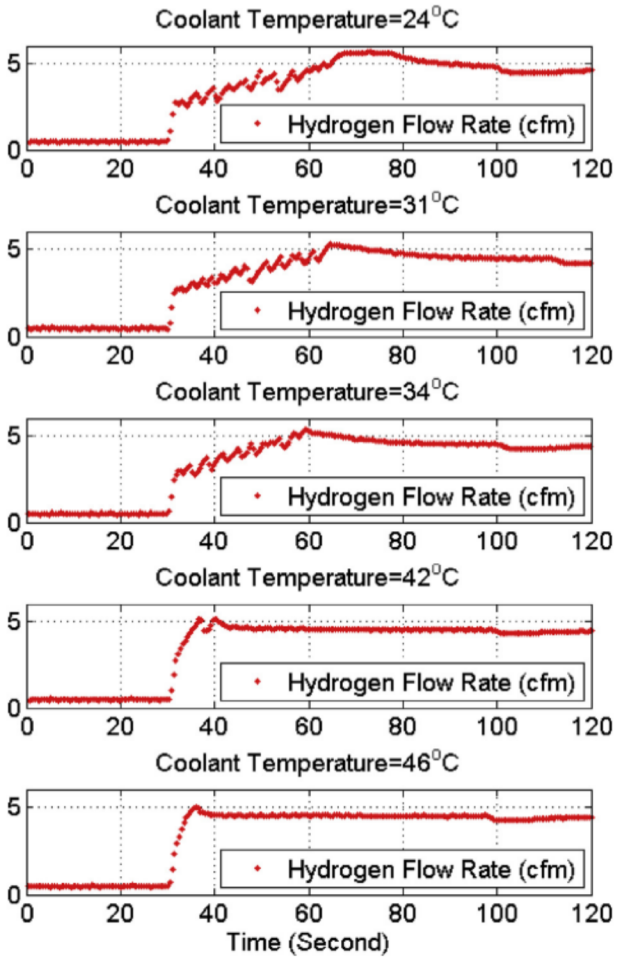

Fig. 15 – The hydrogen flow rate of the PEMFC system operating at various coolant temperatures, the external load changes from 0 kW to 9 kW at t = 30 s.

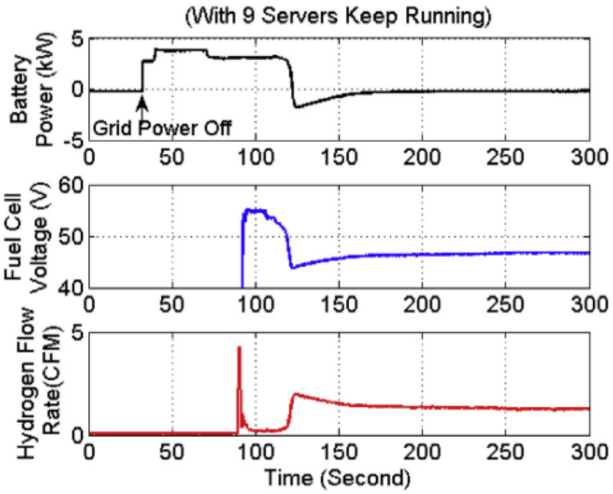

Fig. 16 – Battery power, fuel cell voltage and hydrogen flow rate responses to the startup process.

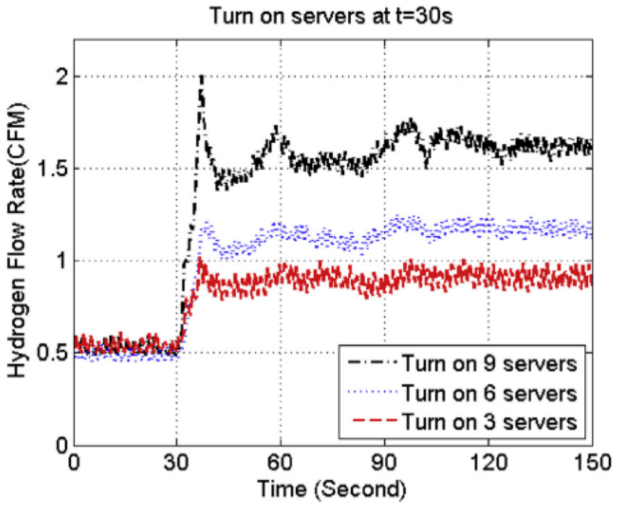

Fig. 18 – Hydrogen flow rate transient response to servers' dynamic operation.

ultracapacitor, Li–ion battery, Lead–acid battery, Ni–Cd battery, and Ni–MH battery are simulated and the capacity and the cost for the in-rack hybrid system are evaluated.

Battery and ultracapacitor model development and verification

To analyze the implications of the transient behavior on various energy storage devices, a detailed model comprised of the various energy storage devices and the measured load change dynamics is developed in MATLAB/Simulink®. Generic equivalent circuit models of the non-linear battery that is implemented in SimPowerSystems™ in MATLAB/Simulink® were used in this study. Based on the discharge characteristics, all the parameters of the equivalent circuit can be

Table 3 – Battery power and energy need for the servers' dynamic operation.

External load	Energy required from battery during transient (kWh)	Average battery power required during transient (kW)	Peak power (kW)
3 servers	0.0006	0.3813	2.3419
6 servers	0.0012	0.7048	3.3118
9 servers	0.0014	0.9203	3.0149

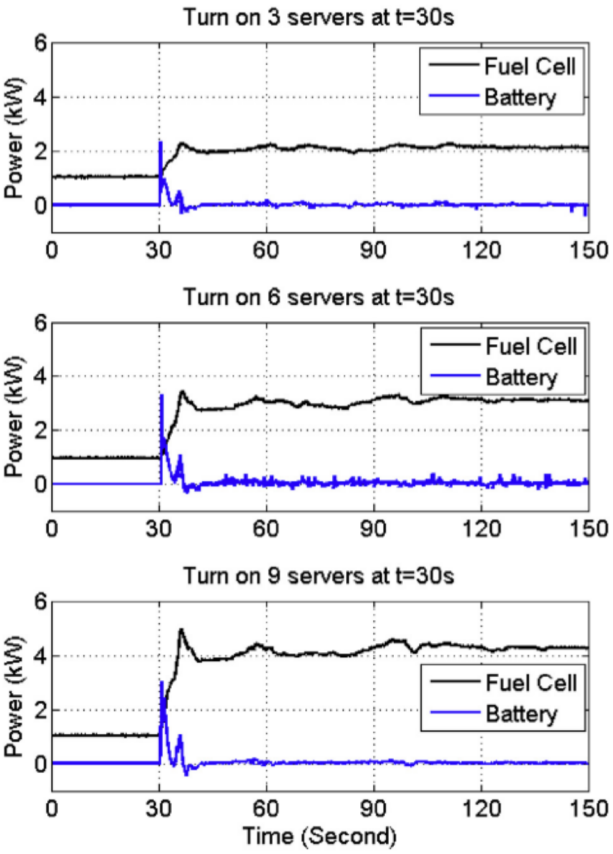

Fig. 17 – Battery power and fuel cell power responses to servers' dynamic operation.

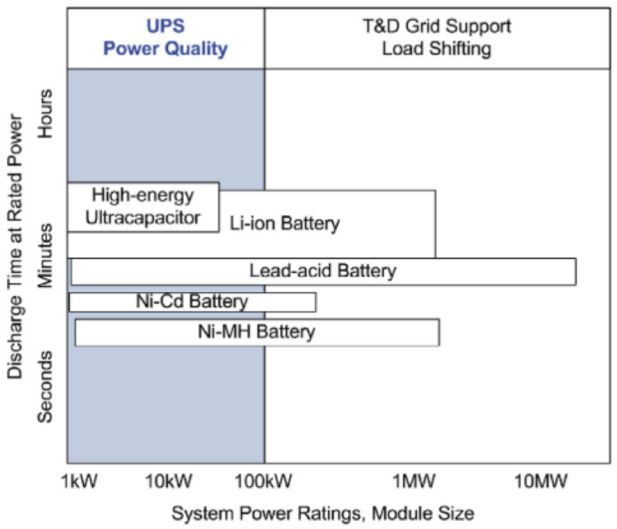

Fig. 19 – Comparison of discharge time and power rating for various energy storage technologies [19].

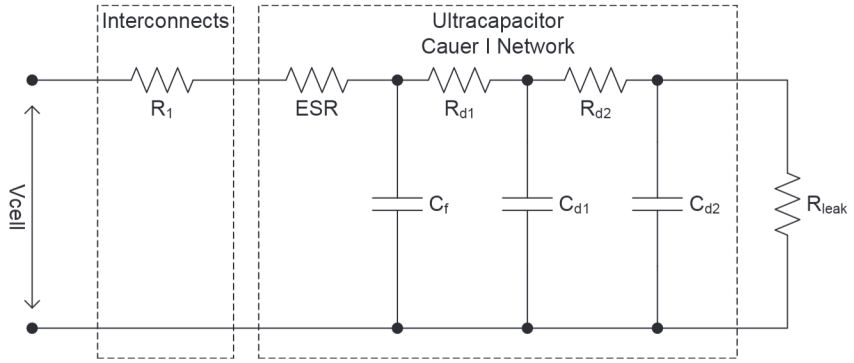

Fig. 20 – Equivalent circuit model of ultracapacitor.

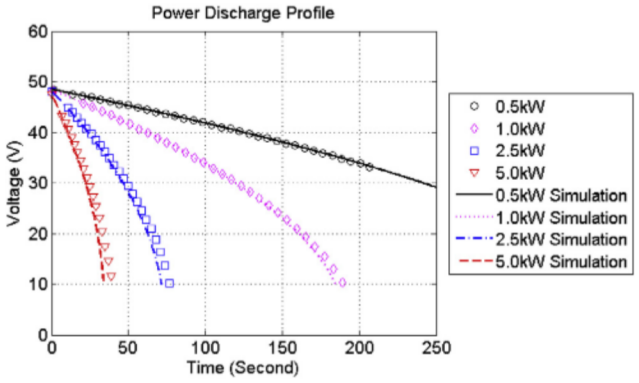

Fig. 21 – 48 V module (BMOD0165-P048) ultracapacitor model verification.

modified to represent a particular battery type. In this study, a 48 V battery module using Li–ion battery, Lead–acid battery, Ni–Cd battery, and Ni–MH battery technology are simulated. A 48 V ultracapacitor module based upon a different equivalent circuit is also developed and verified. The equivalent ultracapacitor circuit used in the current model is shown in Fig. 20. The single resistor of R1 represents the terminal interconnect resistance, while the resistor ESR represents the equivalent series resistance of the combined effect of interconnects, metal foil current collectors and interfacial resistance of the carbon electrodes. Compared to the most commonly used classical RC equivalent circuit model, the Cauer I network used in this study gives more insight into the origins of the three time constant approximations of an ultracapacitor model [45]. The branches of ESR-C_f, R_{d1}-C_{d1}, and R_{d2}-C_{d2} account for the highly distributed effects of carbon matte resistance, ionic conduction, and Helmholtz double layer capacitances existing at "macro", "meso" and "micro" pores in the electrodes, respectively [45]. The resistor R_{leak} represents the self-discharge behavior of ultracapacitor, and which is an important factor to determine the duration time of stored energy at open circuit [46]. Dynamic simulations are performed in MATLAB/Simulink® environment with SimPowerSystems™, and the simulation results were compared to the data obtained from an ultracapacitor manufacturer (Maxwell®) as shown in Fig. 21. Constant power tests are commonly used for the characterization of electric storage devices and generators. For an ultracapacitor, the common experimental procedure is discharging the ultracapacitor with constant power between two voltage limits of V_{rated} and 0.5 V_{rated} in order to measure the specific energy that any particular ultracapacitor can supply as function of discharge power [47]. It can be seen from Fig. 21 that the results obtained by the current simulation are in good agreement with the manufacturer's data for the 48 V ultracapacitor module (BMOD0165-P048, rated capacity 165F, rated voltage 48 V, and stored energy 53 Wh) in the range of 24 V–48 V at various constant power output settings.

Discharging and charging profiles and storage sizing

The transient response of the various energy storage devices to the startup load change is simulated. The startup load change profile for the simulation was comprised of the worst oscillation transient obtained from Fig. 13 (coolant temperature = 24 °C) and a 9 kW power spike which lasts 5 ms to simulate the instantaneous power spike when servers are turned on. The initial state of charge of all devices simulated is set to 90%, and at t = 30 s the devices start to discharge according to the startup load change profile. And at t = 120s, the devices are being charged by 1 kW constant power input (representing 10% of the rated power of the PEMFC system) until the state of the charge returns to the initial state. It is assumed that the load could utilize 48VDC output from the

Table 4 – Minimum battery capacity required to supply the power during the worst transient.

Battery type	Rated voltage	Minimum capacity without the start-up power spike	Minimum capacity with the start-up power spike	Capacity increased (%)
Lithium-ion	48 V	254.4 Wh	336 Wh	32.1%
Lead acid		345.6 Wh	374.4 Wh	8.3%
Ni–Cd		249.6 Wh	326.4 Wh	30.8%
Ni–MH		244.8 Wh	321.6 Wh	31.4%

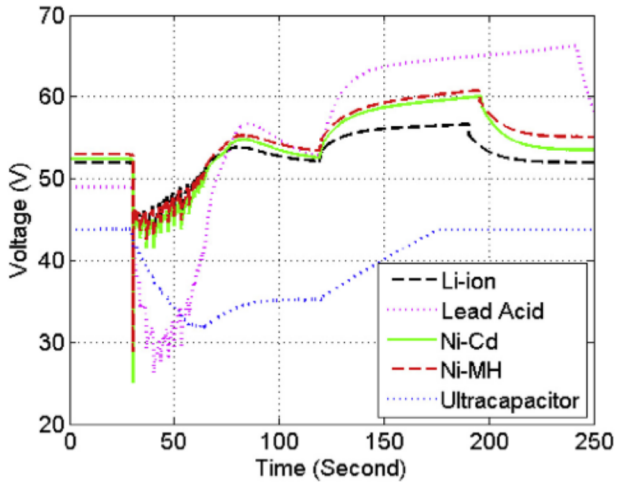

Fig. 22 – Simulated voltage of various energy storage devices during discharging and charging processes.

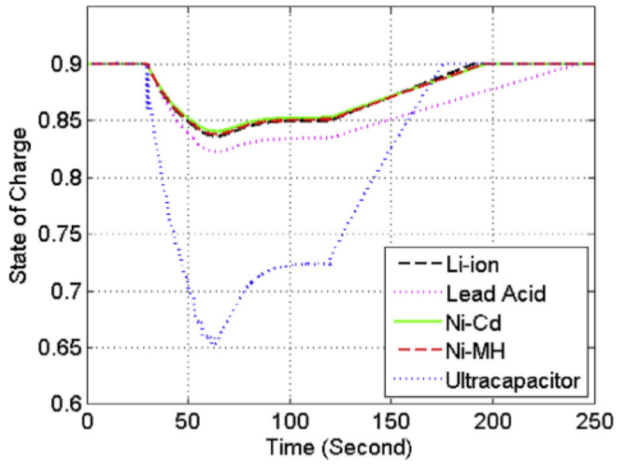

Fig. 23 – Simulated state of charge of various energy storage devices during discharging and charging processes.

energy storage module directly and that there are no conversion/inversion losses. The minimum capacity of each battery type was determined by the simulation and is summarized in Table 4. Note that the impact that the startup 9 kW power spike, which lasts 5 ms, has on the minimum capacity of the battery is also evaluated and presented in Table 4. Though the total energy required from the power spike is relatively low, the high power requirement must to be accommodated by increasing the battery capacity. That is, both energy and power demand dynamics affect battery sizing requirements.

Fig. 22 shows the voltage response of the devices simulated during the discharging and charging process. The battery used in this simulation is a 48 V module with the minimum capacity required to meet the oscillation transient and the startup power spike as listed in Table 4. The ultracapacitor used in this simulation is a 48 V ultracapacitor module (BMOD0165-P048, 165F, 53 Wh). For all the batteries, the voltage dropped sharply towards the cut-off voltage at the beginning of the transient due to the 9 kW power spike. In contrast, the 9 kW power spike only lead to a small voltage drop in the ultracapacitor voltage. It is noted that during the oscillation transient, the voltage response of the ultracapacitor is relatively linear compared to the battery voltage discharging profiles. The state of charge (SOC) of all devices simulated is presented in Fig. 23. The SOC simulation results indicate that to supply the additional power to compensate for the load dynamics that the fuel cell cannot meet, the variation of SOC states for the Li–ion battery, Ni–Cd battery and Ni–MH battery are almost identical. Charging with 1 kW constant power, the ultracapacitor uses the shortest amount of time to recover to the original SOC, while the charging duration for lead acid battery is twice as long as that of the ultracapacitor. The charging duration of various energy storage devices using 2 kW constant power was also simulated and the results are summarized and compared in Table 5.

Although it is not the intent of this paper to provide detailed cost comparisons, a few comments and evaluations are produced as shown in Table 6. The energy cost ($/kWh) of various types of batteries and ultracapacitors are garnered from multiple sources [22,48–52], and the cost of the battery component for the in-rack hybrid system is projected for each case. In addition, the typical cycle life of each battery type and ultracapacitor are also compared [48,49,52]. To be integrated into the in-rack hybrid system, the 48 V ultracapacitor has the smallest capacity and much better cycle life, however, the cost is relatively high. Regardless of the cycle life, the Ni–MH battery and the Lead acid battery are found to be the most cost effective energy storage devices for the hybrid system. Depending upon the system design requirements, constraints such as maximum discharge rate, cutoff voltage, maximum capacity and cost of the battery need to be taken into account when sizing and optimizing the batteries in a hybrid fuel cell system.

Table 5 – Charging duration of various energy storage devices after the 0–9 kW cold step load transient discharging process.

Energy storage type	Rated voltage	Capacity (kWh)	Time for battery back to the original SOC (s)	
			Charging power = 1 kW (10% of FC rated power)	Charging power = 2 kW (20% of FC rated power)
Li-ion	48 V	0.336	70.3 s	36.9 s
Lead acid		0.374	122.4 s	68.8 s
Ni–Cd		0.326	76.6 s	40.8 s
Ni–MH		0.322	75.4 s	39.9 s
Ultracapacitor		0.053	55.5 s	27.0 s

Table 6 – Comparison of energy storage devices cost and typical cycle life.

	Cost ($/kWh)	Size (kWh)	Cost (with 50% power margin for all batteries)	Typical cycle life
Li-ion	$950–$3600 [22]	0.336	$638–$2419	1000–30,000[a] [48]
Lead acid	$400–$950 [22]	0.374	$299–$711	500–2000[a] [48]
Ni–Cd	$500–$1424 [50]	0.326	$326–$928	750–1500 [51,52]
Ni-MH	$200–$1000 [49]	0.322	$129–$644	500–1250 [49,52]
Ultracapacitor BMOD0165-P048		0.053	$1621	1,000,000[b] [53]

[a] Numbers of cycles to failure, at 80% depth of discharge [48].
[b] Projected Cycle Life at 25 °C. Cycle using specified test current per waveform at 50% depth of discharge [53].

Summary and conclusions

In this paper, a direct power generation method that places a hybrid system (comprised of a 12 kW PEMFC and battery) at the rack level, only inches from the servers, is tested and characterized. By using this design, the power distribution system in the data center and the grid outside of the data center can potentially be eliminated. The steady state performance and the transient response of the PEMFC system and the battery in response to AC loads and real server loads have been evaluated and characterized. The PEMFC system is found to respond quickly and reproducibly to load changes directly from the server rack. Peak efficiency of 55.2% in a single server rack can be achieved. The effect of fuel cell coolant temperature on the hybrid system transient behavior is also captured and evaluated. The ramp rate and dynamic response time of the system characterized in this study can be used to develop control strategies to enable dynamic load following capability. Further, simulations and analysis of various types of energy storage devices for the hybrid system were carried out. The battery transient responses obtained from the experiments were used to design the battery/energy storage size for the hybrid system.

Acknowledgments

The authors would like to thank Richard Hack and Brendan Shaffer from Advanced Power and Energy Program, University of California, Irvine, for their technical support.

REFERENCES

[1] DOE. Data Center Energy Consumption Trend n.d. http://energy.gov/eere/femp/articles/data-center-energy-consumption-trends.
[2] Sverdlik Y. eBay's Utah data center offers a glimpse into the future n.d.
[3] Zhao L, Brouwer J, James S, Peterson E, Wang D, Liu J. Fuel cell powered data centers: in-rack DC generation. ECS Trans 2016;71:131–9. http://dx.doi.org/10.1149/07101.0131ecst.
[4] Zhao L, Brouwer J, James S, Siegler J, Peterson E, Kansal A, et al. Servers powered by a 10kW in-rack proton exchange membrane fuel cell system. In: ASME 2014 12th Int Conf Fuel Cell Sci Eng Technol., ASME; 2014. http://dx.doi.org/10.1115/FuelCell2014-6331. V001T02A002.
[5] eBay turns on first fuel cell powered data centre, has Bloom tech. Fuel Cells Bull 2013;2013:3–4. http://dx.doi.org/10.1016/S1464-2859(13)70341-9.
[6] Apple doubles fuel cell capacity at {NC} data centre with Bloom. Fuel Cells Bull 2013;2013:5. http://dx.doi.org/10.1016/S1464-2859(13)70011-7.
[7] Guizzi GL, Manno M. Fuel cell-based cogeneration system covering data centers' energy needs. Energy 2012;41:56–64. http://dx.doi.org/10.1016/j.energy.2011.07.030.
[8] Xu D, Qu M. Energy, environmental, and economic evaluation of a {CCHP} system for a data center based on operational data. Energy Build 2013;67:176–86. http://dx.doi.org/10.1016/j.enbuild.2013.08.021.
[9] Hagstotz F. Permanent premium power for data centers – the fuel cell power station type HotModule. In: Telecommun. Energy Conf. 2007 INTELEC 2007 29th Int; 2007. p. 11–4. http://dx.doi.org/10.1109/INTLEC.2007.4448727.
[10] Haynes C. Simulating process settings for unslaved {SOFC} response to increases in load demand. J Power Sources 2002;109:365–76. http://dx.doi.org/10.1016/S0378-7753(02)00088-5.
[11] Mueller F, Jabbari F, Gaynor R, Brouwer J. Novel solid oxide fuel cell system controller for rapid load following. J Power Sources 2007;172:308–23. http://dx.doi.org/10.1016/j.jpowsour.2007.05.092.
[12] Pukrushpan JT, Stefanopoulou AG, Peng H. Modeling and control for PEM fuel cell stack system. Am Control Conf 2002 Proc 2002 2002;4:3117–22. http://dx.doi.org/10.1109/ACC.2002.1025268.
[13] Auld AE, Mueller F, Smedley KM, Samuelsen S, Brouwer J. Applications of one-cycle control to improve the interconnection of a solid oxide fuel cell and electric power system with a dynamic load. J Power Sources 2008;179:155–63. http://dx.doi.org/10.1016/j.jpowsour.2007.12.072.
[14] Kim S, Shimpalee S, Van Zee JW. The effect of stoichiometry on dynamic behavior of a proton exchange membrane fuel cell (PEMFC) during load change. J Power Sources 2004;135:110–21. http://dx.doi.org/10.1016/j.jpowsour.2004.03.060.
[15] Yan Q, Toghiani H, Causey H. Steady state and dynamic performance of proton exchange membrane fuel cells (PEMFCs) under various operating conditions and load changes. J Power Sources 2006;161:492–502. http://dx.doi.org/10.1016/j.jpowsour.2006.03.077.
[16] Bezmalinovic D, Barbir F. Fuel cell stack operation with low cathode stoichiometry with cells or sections fed in series. In: ECS Trans., ECS; 2009. p. 2009–17. http://dx.doi.org/10.1149/1.3210757.
[17] Zheng Z, Petrone R, Pera MC, Hissel D, Becherif M, Pianese C. Diagnosis of a commercial PEM fuel cell stack via incomplete spectra and fuzzy clustering. In: IECON Proc (Industrial Electron Conf.); 2013. p. 1595–600. http://dx.doi.org/10.1109/IECON.2013.6699371.

[18] Burke A. Batteries and ultracapacitors for electric, hybrid, and fuel cell vehicles. Proc IEEE 2007;95:806–20. http://dx.doi.org/10.1109/JPROC.2007.892490.
[19] Dunn B, Kamath H, Tarascon J-M. Electrical energy storage for the grid: a battery of choices. Science 2011;334:928–35. http://dx.doi.org/10.1126/science.1212741.
[20] Latha K, Umamaheswari B, Rajalakshmi N, Dhathathreyan KS. Investigation of various operating modes of fuelcell/ultracapacitor/multiple converter based hybrid system. 2013 IEEE 10th Int Conf Power Electron Drive Syst IEEE 2013:65–71. http://dx.doi.org/10.1109/PEDS.2013.6526990.
[21] Mesbahi T, Rizoug N, Bartholomeüs P, Moigne P Le. A new energy management strategy of a battery/supercapacitor hybrid energy storage system for electric vehicular applications. 7th IET Int Conf Power Electron Mach Drives (PEMD 2014) 2014;1:8–10. http://dx.doi.org/10.1049/cp.2014.0442.
[22] Rastler D. EPRI project manager electricity energy storage technology options disclaimer of warranties and limitation of liabilities. 2010.
[23] Uzunoglu M, Alam MS. Dynamic modeling, design, and simulation of a combined PEM fuel cell and ultracapacitor system for stand-alone residential applications. IEEE Trans Energy Convers 2006;21:767–75. http://dx.doi.org/10.1109/TEC.2006.875468.
[24] Gao W. Performance comparison of a fuel cell-battery hybrid powertrain and a fuel cell-ultracapacitor hybrid powertrain. IEEE Trans Veh Technol 2005;54:846–55. http://dx.doi.org/10.1109/TVT.2005.847229.
[25] Zandi M, Payman A, Martin J-P, Pierfederici S, Davat B, Meibody-Tabar F. Energy management of a fuel cell/supercapacitor/battery power source for electric vehicular applications. IEEE Trans Veh Technol 2011;60:433–43. http://dx.doi.org/10.1109/TVT.2010.2091433.
[26] Guo Y-F, Chen H-C, Wang F-C. The development of a hybrid PEMFC power system. Int J Hydrogen Energy 2015;40:4630–40. http://dx.doi.org/10.1016/j.ijhydene.2015.01.169.
[27] Saadi A, Becherif M, Hissel D, Ramadan HS. Dynamic modeling and experimental analysis of PEMFCs: a comparative study. Int J Hydrogen Energy 2016. http://dx.doi.org/10.1016/j.ijhydene.2016.07.180.
[28] Liu Z, Li L, Ding Y, Deng H, Chen W. Modeling and control of an air supply system for a heavy duty PEMFC engine. Int J Hydrogen Energy 2016;41:16230–9. http://dx.doi.org/10.1016/j.ijhydene.2016.04.213.
[29] Mayur M, Strahl S, Husar A, Bessler WG. A multi-timescale modeling methodology for PEMFC performance and durability in a virtual fuel cell car. Int J Hydrogen Energy 2015;40:16466–76. http://dx.doi.org/10.1016/j.ijhydene.2015.09.152.
[30] Haddad D, Oulmi K, Benmoussa H, Aouachria Z, Bourmada N. Transport phenomena effect on the performance of proton exchange membrane fuel cell (PEMFC). Int J Hydrogen Energy 2013;38:8550–6. http://dx.doi.org/10.1016/j.ijhydene.2012.11.011.
[31] Chen X, Gong G, Wan Z, Luo L, Wan J. Performance analysis of 5 kW PEMFC-based residential micro-CCHP with absorption chiller. Int J Hydrogen Energy 2015;40:10647–57. http://dx.doi.org/10.1016/j.ijhydene.2015.06.139.
[32] Geraldo de Melo Furtado J, Gatti GC, Serra ET, Anibal de Almeida SC. Performance analysis of a 5 kW PEMFC with a natural gas reformer. Int J Hydrogen Energy 2010;35:9990–5. http://dx.doi.org/10.1016/j.ijhydene.2010.02.042.
[33] Webb D, Møller-Holst S. Measuring individual cell voltages in fuel cell stacks. J Power Sources 2001;103:54–60. http://dx.doi.org/10.1016/S0378-7753(01)00831-X.
[34] Mulder G, De Ridder F, Coenen P, Weyen D, Martens A. Evaluation of an on-site cell voltage monitor for fuel cell systems. Int J Hydrogen Energy 2008;33:5728–37. http://dx.doi.org/10.1016/j.ijhydene.2008.07.017.
[35] Li Y, Zhao X, Liu Z, Li Y, Chen W, Li Q. Experimental study on the voltage uniformity for dynamic loading of a PEM fuel cell stack. Int J Hydrogen Energy 2015;40:7361–9. http://dx.doi.org/10.1016/j.ijhydene.2015.04.058.
[36] Qu S, Li X, Hou M, Shao Z, Yi B. The effect of air stoichiometry change on the dynamic behavior of a proton exchange membrane fuel cell. J Power Sources 2008;185:302–10. http://dx.doi.org/10.1016/j.jpowsour.2008.06.080.
[37] Wang Y-X, Xuan D-J, Kim Y-B. Design and experimental implementation of time delay control for air supply in a polymer electrolyte membrane fuel cell system. Int J Hydrogen Energy 2013;38:13381–92. http://dx.doi.org/10.1016/j.ijhydene.2013.06.040.
[38] Hu J, Xu L, Li J, Fang C, Cheng S, Ouyang M, et al. Model-based estimation of liquid saturation in cathode gas diffusion layer and current density difference under proton exchange membrane fuel cell flooding. Int J Hydrogen Energy 2015;40:14187–201. http://dx.doi.org/10.1016/j.ijhydene.2015.09.005.
[39] Shimpalee S, Lee W-K, Van Zee JW, Naseri-Neshat H. Predicting the transient response of a serpentine flow-field PEMFC: II: normal to minimal fuel and AIR. J Power Sources 2006;156:369–74. http://dx.doi.org/10.1016/j.jpowsour.2005.05.074.
[40] Raceanu M, Marinoiu A, Culcer M, Varlam M, Bizon N. Preventing reactant starvation of a 5 kW PEM fuel cell stack during sudden load change. Proc 2014 6th Int Conf Electron Comput Artif Intell IEEE 2014:55–60. http://dx.doi.org/10.1109/ECAI.2014.7090147.
[41] Rajalakshmi N, Dhathathreyan KS. Catalyst layer in PEMFC electrodes—fabrication, characterisation and analysis. Chem Eng J 2007;129:31–40. http://dx.doi.org/10.1016/j.cej.2006.10.035.
[42] Misran E, Mat Hassan NS, Wan Daud WR, Majlan EH, Rosli MI. Electrochemical properties of a PEMFC operating with saturated hydrogen and dry air. Int J Hydrogen Energy 2013;38:9395–400. http://dx.doi.org/10.1016/j.ijhydene.2012.12.122.
[43] Kunusch C, Puleston PF, Mayosky MA, Moré JJ. Characterization and experimental results in PEM fuel cell electrical behaviour. Int J Hydrogen Energy 2010;35:5876–81. http://dx.doi.org/10.1016/j.ijhydene.2009.12.123.
[44] Perez-Page M, Perez-Herranz V. Effect of the operation and humidification temperatures on the performance of a PEM fuel cell stack. ECS Trans 2009;25:733–45. http://dx.doi.org/10.1149/1.3210625. ECS.
[45] Penella-López MT, Gasulla-Forner M. Primary batteries and storage elements. Powering auton. Sensors, Dordrecht: Springer Netherlands; 2011. p. 41–80. http://dx.doi.org/10.1007/978-94-007-1573-8_4.
[46] Vural B, Uzunoglu M, Erdinc O, Onar OC. A dynamic ultra-capacitor model for vehicular applications. 2009 Int Conf Clean Electr Power IEEE 2009:595–8. http://dx.doi.org/10.1109/ICCEP.2009.5211994.
[47] Lajnef W, Vinassa J-M, Briat O, Azzopardi S, Woirgard E. Characterization methods and modelling of ultracapacitors for use as peak power sources. J Power Sources 2007;168:553–60. http://dx.doi.org/10.1016/j.jpowsour.2007.02.049.
[48] Battke B, Schmidt TS, Grosspietsch D, Hoffmann VH. A review and probabilistic model of lifecycle costs of stationary batteries in multiple applications. Renew Sustain Energy Rev 2013;25:240–50. http://dx.doi.org/10.1016/j.rser.2013.04.023.

[49] Graham R. Market feasibility for nickel metal hyride and other advanced electric vehicle batteries in selected stationary applications. n.d.
[50] Steward D, Saur G, Penev M, Ramsden T. Lifecycle cost analysis of hydrogen versus other technologies for electrical energy storage. 2009.
[51] Industrial Ni-Cd batteries standard range technical manual. 2009.
[52] Whitaker JC. The electronics handbook. CRC Press; 2005.
[53] Datasheet 48V modules features and benefits* n.d.